Progress In Electromagnetics Research, Vol. 140, 719–732, 2013

FAR-FIELD RECONSTRUCTION FROM NEAR-FIELD DATA ACQUIRED VIA A FAST SPHERICAL SPIRAL SCAN: EXPERIMENTAL EVIDENCES

Francesco D'Agostino, Flaminio Ferrara, Claudio Gennarelli*, Rocco Guerriero, and Massimo Migliozzi

Dipartimento di Ingegneria Industriale, University of Salerno, via Giovanni Paolo II, Fisciano, Salerno 132-84084, Italy

Abstract—A probe-compensated near-field-far-field (NF-FF) transformation with spherical spiral scanning, which makes possible to lower the number of needed measurements, as well as the time required for the data acquisition when characterizing quasi-planar antennas, is experimentally verified in this paper. Such a technique, based on the nonredundant representation of electromagnetic fields, has been achieved by properly applying the unified theory of spiral scans for nonspherical antennas and adopting a very flexible source modelling, formed by two circular "bowls" with the same aperture diameter but different bending radii. A two-dimensional optimal sampling interpolation formula allows one to reconstruct the NF data at any point on the measurement sphere and, in particular, at those required by the classical NF-FF transformation with spherical scanning. The reported NF and FF reconstructions, obtained from the nonredundant samples acquired on the spiral, assess the accuracy of the proposed technique.

1. INTRODUCTION

Near-field-far-field (NF-FF) transformation techniques represent nowadays a very useful tool to overcome those problems and limitations, which make impossible or impractical the measurement of the antenna radiation patterns on a conventional FF range [1–3]. The antenna measurement people community has spent over the years many efforts to satisfy the ever growing demand of innovative solutions to the open issues [4]. Among them, the reduction of the time needed

Received 2 May 2013, Accepted 22 June 2013, Scheduled 2 July 2013

* Corresponding author: Claudio Gennarelli (gennar@diiie.unisa.it).

for the NF data acquisition is assuming a significant importance, since such a time is currently very much greater than that required to perform the transformation. This challenge can be tackled by decreasing the number of the NF data to be collected and/or by making faster the acquisition of each NF value. A convenient way of reducing the number of the needed NF data is offered by the nonredundant sampling representations of electromagnetic (EM) fields [5, 6]. As a matter of fact, the EM fields radiated by finite size sources enclosed in a convex domain $\mathcal{D}$, bounded by a surface Σ with rotational symmetry and observed on a regular surface $\mathcal{M}$ external to $\mathcal{D}$ and having the same symmetry, can be always represented by a finite number of NF data also for an unbounded observation domain, provided that a proper phase factor is extracted from the field expression and proper parameterizations are adopted to describe $\mathcal{M}$. It has been so possible to develop efficient NF-FF transformation techniques with planar [7–9], cylindrical [10, 11], and spherical [12, 13] scannings, which generally require a number of NF data remarkably lower than the standard ones. In fact, the NF data needed by the corresponding standard NF-FF transformation [14–16] are accurately recovered by interpolating the minimum set of measurements via optimal sampling interpolation (OSI) expansions.

When the NF data acquisition is made, as suggested by Yaccarino et al. in [17], by means of continuous and synchronized movements of the positioning systems of the probe and antenna under test (AUT), then a faster NF scanning results. This suggestion has enabled the development of the innovative spiral scanning techniques [18–29]. Besides the use of continuous movements, the drastic time saving characterizing these scanning techniques is due to the significantly reduced number of needed NF data related to the application of the aforementioned nonredundant sampling representations, which can be further lowered if the surface Σ enclosing the AUT fits better its actual shape. Thus, such a number is reduced more and more passing from the quite general spherical AUT modelling for volumetrical antennas to those particularly suitable for AUTs having one or two dimensions very different from the third one. An efficient two-dimensional OSI formula, obtained by choosing the spiral step equal to the sample spacing needed to interpolate the data along a meridian curve (radial line, generatrix, and meridian), allows one to recover the NF data required to perform the NF-FF transformation using the corresponding classical scanning. Moreover, in order to match the advantages of the direct cylindrical NF-FF transformation [30, 31] with those own of the fast helicoidal scan, direct NF-FF transformations with helicoidal scanning, which allow one to

evaluate the antenna far field in any cut plane directly from a minimum set of NF data without interpolating them, have been recently proposed in [32, 33].

Among the NF-FF transformations, that employing the spherical spiral scanning [23–28], as well as that employing the spherical one [12, 13, 16, 34–36], have attracted considerable attention, since they allow the full reconstruction of the AUT radiation pattern, even though the data processing is considerably more complex than that needed by planar and cylindrical NF facilities [1, 2]. In particular, the nonredundant sampling representation on the sphere from samples collected along the spiral and the related OSI expansion have been developed in [23–25] by assuming the AUT as enclosed in the smallest sphere able to contain it and choosing the spiral step equal to the sample spacing required for the interpolation along a meridian. Then, NF-FF transformations with spherical spiral scanning tailored for electrically long or quasi-planar antennas have been proposed in [26–28] by properly applying the unified theory of spiral scans for nonspherical antennas [29]. In particular, a prolate [26] and an oblate [26, 27] ellipsoid have been adopted to model an elongated and a quasi-planar antenna, respectively. Whereas in [28], an elongated AUT has been considered as enclosed in a cylinder ended in two half spheres (rounded cylinder), and a surface formed by two circular bowls with the same aperture diameter but different bending radii (two-bowls modelling) has been used for modelling quasi-planar antennas. Generally, these last two flexible AUT modellings result to be more effective from the data reduction viewpoint than the corresponding ellipsoidal ones, since they are able to fit better the AUT shape by properly setting their geometric parameters.

The NF-FF transformation with spherical spiral scan [28], using the two-bowls modelling (Fig. 1) to shape quasi-planar antennas, is experimentally validated in this paper. The tests have been performed at the Antenna Characterization Lab of University of Salerno, equipped with a roll over azimuth spherical NF facility system, and have fully confirmed the effectiveness of the technique.

2. NONREDUNDANT REPRESENTATION OF THE PROBE VOLTAGE ON A SPHERE FROM SAMPLES COLLECTED ALONG A SPIRAL

In the spherical spiral scanning, the AUT is located at the origin of a spherical coordinate system (r, ϑ, φ) and the field radiated by it is measured by a probe scanning a spiral lying on a spherical surface $\mathcal{M}$ having radius d (Fig. 1). It has been shown [37] that the voltage V

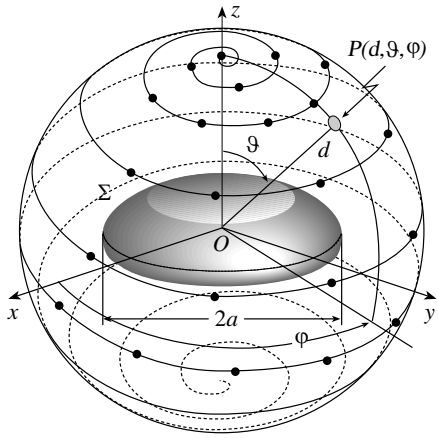

Figure 1. Spherical spiral scanning for a quasi-planar antenna.

measured by a nondirective probe is characterized by the same effective spatial bandwidth of the field and, accordingly, the theoretical results relevant to the nonredundant sampling representation of EM fields [5] can be applied to it. To this end, let us consider the AUT as enclosed in an opportune rotational surface Σ bounding a convex domain $\mathcal{D}$ and an observation curve C on $\mathcal{M}$ described by a proper parameterization $\underline{r} = \underline{r}(\eta)$. Under these hypotheses, the "reduced voltage"

$$\tilde{V}(\eta) = V(\eta)e^{j\psi(\eta)}, \tag{1}$$

obtained by extracting a proper a phase function from the expression of each of the voltages V_1 and V_2 measured by the probe and rotated probe, can be closely approximated by a spatially bandlimited function [5]. The resulting bandlimitation error, which exhibits a step-like behaviour, becomes negligible as the bandwidth exceeds a critical value W_η [5]. As a consequence, such an error can be easily controlled by choosing the bandwidth of the approximating function equal to $\chi' W_\eta$, where χ' is an enlargement bandwidth factor, slightly greater than unity for electrically large antennas.

When the AUT geometry departs from the spherical one, as in the case of an antenna characterized by a quasi-planar geometry, the use of the quite general spherical AUT modelling is not very satisfactory from the data reduction point of view. In such a case, it is convenient for reducing the volumetrical redundancy of the spherical modelling [23–25] to choose the surface Σ enclosing it coincident with that formed by two circular "bowls" with the same aperture diameter $2a$, but lateral bends which can be eventually different to fit the AUT geometry better.

According to the unified theory of spiral scans for nonspherical AUTs [29], heuristically derived by paralleling the rigorous approach based on the use of the spherical AUT modelling [24], a two-dimensional OSI expansion to reconstruct the voltage from a nonredundant number of samples collected by the probe along a spherical spiral can be obtained: a) by choosing the spiral pitch equal to the sample spacing required to interpolate the data along a meridian; b) by developing a nonredundant sampling representation of the probe voltage on the spiral.

In particular, the bandwidth W_η, the parameterization η, and the corresponding phase function ψ, which allow one to fix the sampling representation along a meridian and match the requirement a), are given by [28, 29]:

$$W_\eta = \beta\ell'/2\pi \tag{2}$$

$$\eta = \frac{\pi}{\ell'}\left[R_1 - R_2 + s_1' + s_2'\right] \tag{3}$$

$$\psi = \frac{\beta}{2}\left[R_1 + R_2 + s_1' - s_2'\right] \tag{4}$$

where β is the wavenumber, $\ell' = 2[b + b' + (c + c')\pi/2]$, $b = a - c$, $b' = a - c'$, and the expressions of the distances $R_{1,2}$ and curvilinear abscissae $s'_{1,2}$ change depending on the location of the tangency points $P_{1,2}$, as ϑ varies in the range $[0, \pi]$ (see Fig. 2). Thus, five cases must be considered [28]. Their explicit evaluation is reported in Appendix A for reader's convenience.

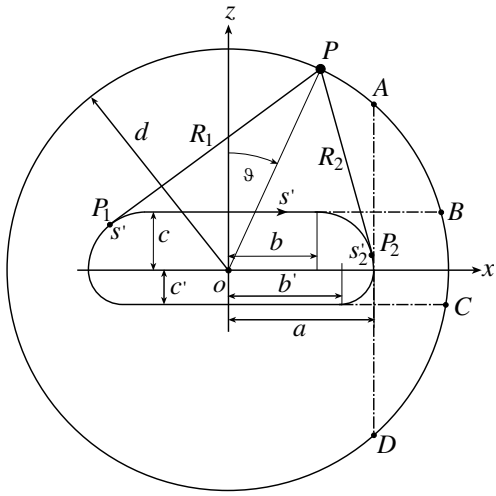

Figure 2. Double bowl modelling.

According to [28, 29], the spiral can be obtained by projecting on the scanning sphere, via the curves at $\eta = \text{const}$, a proper spiral wrapping Σ whose step is equal to the sample spacing $\Delta\eta = 2\pi/(2N'' + 1)$ needed to interpolate the voltage along a meridian. Note that $N'' = \text{Int}(\chi N') + 1$, where $N' = \text{Int}(\chi' W_\eta) + 1$, $\chi > 1$ is an oversampling factor [28, 29], and $\text{Int}(x)$ is the integer part of x.

To match the requirement b) and develop the nonredundant sampling representation of the probe voltage on the spiral, its equations, the parameter ξ to describe it and the phase factor $e^{j\gamma}$ to be multiplied by the voltage expression when interpolating along it have to be determined. The parametric equations of the spiral are given by [28, 29]:

$$\begin{cases} x = d \sin\theta(\eta) \cos\phi \\ y = d \sin\theta(\eta) \sin\phi \\ z = d \cos\theta(\eta) \end{cases} \tag{5}$$

wherein d is the radius of the scanning sphere, ϕ the parameter describing the spiral, and $\eta = k\phi = \phi/(2N'' + 1)$. Note that the spiral angle θ, unlike the zenithal angle ϑ, can assume negative values. The optimal parameter ξ describing the scanning spiral is enforced to be equal to β/W_ξ times the arclength of the projecting point on that wrapping the surface Σ and the related phase function γ is coincident with ψ. Moreover, W_ξ is chosen equal to β/π times the length of the spiral wrapping Σ from pole to pole [28, 29]. Note that the spiral, γ and ξ are such that they coincide with those relevant to the spherical modelling, when the surface Σ leads to a sphere [29].

By taking into account the above results, the voltage at any point Q of the spiral is retrieved via the following OSI formula [28]:

$$\tilde{V}(\xi) = \sum_{m=m_0-p+1}^{m_0+p} \tilde{V}(\xi_m)\, G\left(\xi, \xi_m, \bar{\xi}, M, M''\right) \tag{6}$$

where $m_0 = \text{Int}(\xi/\Delta\xi)$ is the index of the sample nearest (on the left) to Q, $2p$ is the number of the retained samples $\tilde{V}(\xi_m)$, and $\xi_m = m\Delta\xi = 2\pi m/(2M'' + 1)$ with $M'' = \text{Int}(\chi M') + 1$ and $M' = Int(\chi' W_\xi) + 1$. Moreover,

$$G\left(\xi, \xi_m, \bar{\xi}, M, M''\right) = \Omega_M\left(\xi - \xi_m, \bar{\xi}\right) D_{M''}(\xi - \xi_m) \tag{7}$$

is the product of the Dirichlet and Tschebyscheff sampling functions [5]

$$\begin{aligned} D_{M''}(\xi) &= \frac{\sin\left((2M''+1)\,\xi/2\right)}{(2M''+1)\sin(\xi/2)}; \\ \Omega_M(\xi) &= \frac{T_M\left[-1+2\left(\cos(\xi/2)/\cos\left(\bar{\xi}/2\right)\right)^2\right]}{T_M\left[-1+2/\cos^2\left(\bar{\xi}/2\right)\right]} \end{aligned} \tag{8}$$

wherein $T_M(\xi)$ is the Tschebyscheff polynomial of degree $M = M'' - M'$ and $\bar{\xi} = p\Delta\xi$. Note that, when interpolating the voltage nearby the poles ($\vartheta = 0$ and $\vartheta = \pi$), it is necessary to increase the excess bandwidth factor χ' to avoid a serious growth of the bandlimitation error in these zones.

The OSI expansion (6) is employed to recover the "intermediate samples", namely, the voltage values at the intersection points between the spiral and the meridian through the observation point P. Once these samples have been evaluated, the voltage at P on the meridian at φ can be reconstructed via the OSI expansion:

$$\tilde{V}(\eta(\vartheta), \varphi) = \sum_{n=n_0-q+1}^{n_0+q} \tilde{V}(\eta_n)\, G\left(\eta, \eta_n, \bar{\eta}, N, N''\right) \tag{9}$$

wherein, $N = N'' - N'$, $n_0 = \mathrm{Int}[(\eta - \eta_0)/\Delta\eta]$, $2q$ is the number of the retained intermediate samples $\tilde{V}(\eta_n)$,

$$\eta_n = \eta_n(\varphi) = k\varphi + n\Delta\eta = \eta_0 + n\Delta\eta \tag{10}$$

and the other symbols have the same or analogous meaning as in (6). It is so possible to reconstruct the reduced voltage at the points required by the spherical NF-FF transformation [16], as modified in [12, 13]. The voltages which would be measured by the probe at the same points are then obtained by reinserting the corresponding phase factor.

3. EXPERIMENTAL TESTING

This section is devoted to show some experimental results assessing the effectiveness of the described NF-FF transformation with spherical spiral scanning for quasi-planar antennas. They have been performed at the anechoic chamber of the Antenna Characterization Lab of University of Salerno, which is provided with a roll (φ axis) over azimuth (ϑ axis) spherical NF facility supplied by MI Technologies. The chamber, whose dimensions are $8\,\mathrm{m} \times 5\,\mathrm{m} \times 4\,\mathrm{m}$, is covered with pyramidal absorbers ensuring a background noise lower than $-40\,\mathrm{dB}$. An open-ended WR90 rectangular waveguide is used as probe and its response has been collected on a spiral wrapping a sphere having radius $d = 45.2\,\mathrm{cm}$. The amplitude and phase measurements are performed via a vectorial network analyzer. The considered AUT is a X-band flat plate slot array of Rantec Microwave Systems Inc., having a diameter of about 46 cm, located on the plane $z = 0$ of the reference system (Fig. 1). Its optimal working frequencies are: 9.2, 9.3, 9.4, and 9.5 GHz. The reported results are relevant to 9.3 GHz. According to the adopted representation, it has been modelled by a two-bowls modelling having $a = 23.71\,\mathrm{cm}$, $c = 6.45\,\mathrm{cm}$, and $c' = 4.84\,\mathrm{cm}$.

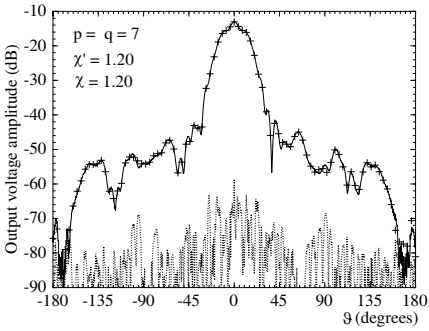

Figure 3. Amplitude of V_1 on the meridian at $\varphi = 0°$. Solid line: measured. Crosses: recovered from NF data acquired via the spherical spiral scanning. Dashed line: reconstruction error.

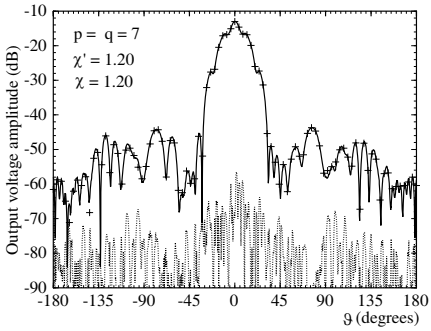

Figure 4. Amplitude of V_2 on the meridian at $\varphi = 90°$. Solid line: measured. Crosses: recovered from NF data acquired via the spherical spiral scanning. Dashed line: reconstruction error.

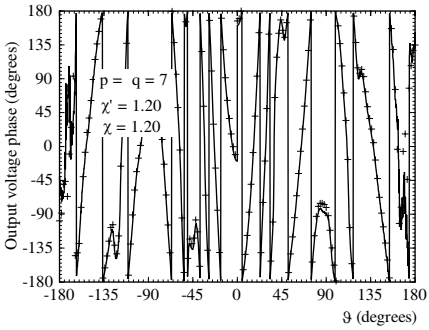

Figure 5. Phase of V_1 on the meridian at $\varphi = 0°$. Solid line: measured. Crosses: recovered from NF data acquired via the spherical spiral scanning.

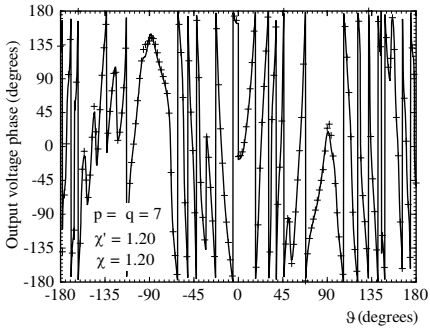

Figure 6. Phase of V_2 on the meridian at $\varphi = 90°$. Solid line: measured. Crosses: recovered from NF data acquired via the spherical spiral scanning.

The effectiveness of the two-dimensional OSI expansion is assessed by comparing in Figs. 3 and 4 the amplitudes of the recovered voltages V_1 and V_2 relevant to the meridians at $\varphi = 0°$ and $\varphi = 90°$, respectively, with those directly acquired on the same meridians. The corresponding reconstruction errors are reported in the same figures, whereas the comparisons between the phases of the reconstructed voltages and those directly measured are shown in Figs. 5 and 6. As can be seen, a very good agreement between the reconstructed voltages (crosses) and the measured ones (solid line) results save for the peripheral zone (below about $-60\,\mathrm{dB}$), wherein a small error, imputable to the noise

and the residual reflections from the anechoic chamber walls, is present. It is worthy to note that a bandwidth factor χ' such that the sample spacing is reduced by a factor 7 has been adopted in the zones of the spherical spiral specified by the 30 samples around the poles, in order to reduce the interpolation error nearby them.

At last, the FF patterns in the principal planes E and H reconstructed from the NF set of measurements acquired through the spherical spiral scan are compared in Figs. 7 and 8 with those (references) obtained from the NF data directly measured on the classical spherical grid. In both the cases, the software package MI-3000 has been used to get the FF patterns. These plots are shown together with the reconstruction error, in order to appreciate the error levels. As can be seen, the reconstructions are very accurate, thus fully confirming the effectiveness of the approach. Quite analogous results (not reported here for brevity) have been obtained for other working frequencies.

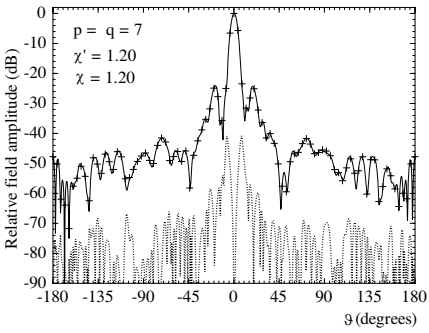

Figure 7. E-plane pattern. Solid line: reference. Crosses: recovered from NF data acquired via the spherical spiral scanning. Dashed line: reconstruction error.

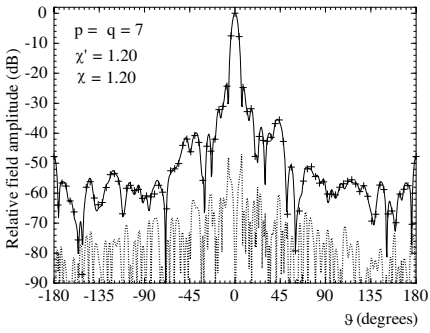

Figure 8. H-plane pattern. Solid line: reference. Crosses: recovered from NF data acquired via the spherical spiral scanning. Dashed line: reconstruction error.

Note that the number of employed samples is 4 408, significantly less than those (6 392 and 7 320) required by the NF-FF transformation [23, 24] based on the spherical AUT modelling and by the MI software package implementing the classical NF-FF transformation with spherical scanning [16], respectively. In particular, the number of "regular samples" at spacing $\Delta\xi$ is 4 048, whereas the number of "extra samples" at reduced spacing is 360.

For what concerns the time needed for the NF data acquisition, the proposed technique is certainly quicker than the traditional one, if the

acquisition is performed by continuous and synchronized movements of the positioning systems [17]. From the computational viewpoint, an additional time is required by the OSI algorithm to reconstruct the NF data needed to perform the classical NF-FF transformation from the nonredundant ones acquired along the spiral. In any case, such a time is many order of magnitude smaller than that needed for the NF data acquisition. For instance, the reconstruction process has taken in the considered case a CPU time of about 2.3 seconds on a PC equipped with an Intel Core 2 Duo @ 3.33 GHz.

4. CONCLUSIONS

An experimental validation of the NF-FF transformation technique with spherical spiral scanning suitable for quasi-planar antennas and using a two-bowls modelling of the AUT has been provided in this paper. The very good agreements found both in the near-field and in the far-field reconstructions confirm also from the experimental viewpoint the validity of such an innovative transformation, which allows a drastic reduction of the measurement time by retaining the accuracy of the classical spherical one. It is worthy to note that the proposed technique, as well as all those using the spiral scannings, allow also the frequency extension of existing near-field ranges, since both measurement axes are used simultaneously hence reducing the effect of backlash.

APPENDIX A. EVALUATION OF $R_{1,2}$ AND $S'_{1,2}$ AS FUNCTION OF ϑ

The explicit evaluation of the distances $R_{1,2}$ of the observation point P from the tangency points $P_{1,2}$ and their curvilinear abscissae $s'_{1,2}$ in (3) and (4) is reported in the following. Their expressions change depending on the location of the points $P_{1,2}$(see Fig. 2) and, accordingly, five cases must be considered for ϑ ranging in $[0, \pi]$.

When $0 \leq \vartheta \leq \vartheta_A = \sin^{-1}(a/d)$, it results:

$$R_1 = \sqrt{d^2 + b^2 + 2bd\sin\vartheta - c^2}; \quad s'_1 = -(b + c\alpha_1) \tag{A1}$$

$$\alpha_1 = \tan^{-1}(R_1/c) - \tan^{-1}[(b + d\sin\vartheta)/d\cos\vartheta] \tag{A2}$$

$$R_2 = \sqrt{d^2 + b^2 - 2bd\sin\vartheta - c^2}; \quad s'_2 = b + c\alpha_2 \tag{A3}$$

$$\alpha_2 = \tan^{-1}(R_2/c) - \tan^{-1}[(b - d\sin\vartheta)/d\cos\vartheta] \tag{A4}$$

When $\vartheta_A < \vartheta \leq \vartheta_B = \cos^{-1}(c/d)$, R_1, s'_1, and α_1 are again given by (A1) and (A2), whereas it results:

$$R_2 = \sqrt{d^2 + b'^2 - 2b'd\sin\vartheta - c'^2}; \quad s'_2 = b + c(\pi/2) + c'\alpha_2 \tag{A5}$$

$$\alpha_2 = \tan^{-1}\left(R_2/c'\right) - \tan^{-1}\left[d\cos\vartheta/\left(d\sin\vartheta - b'\right)\right] \quad \text{(A6)}$$

When $\vartheta_B < \vartheta \leq \vartheta_C = \pi - \cos^{-1}(c'/d)$, R_2, s'_2, and α_2 are again given by (A5) and (A6), whereas it results:

$$R_1 = \sqrt{d^2 + b^2 - 2bd\sin\vartheta - c^2}; \quad s'_1 = b + c(\alpha_1 + \pi/2) \quad \text{(A7)}$$

$$\alpha_1 = -\tan^{-1}(R_1/c) - \tan^{-1}\left[d\cos\vartheta/(d\sin\vartheta - b)\right] \quad \text{(A8)}$$

When $\vartheta_C < \vartheta \leq \vartheta_D = \pi - \sin^{-1}(a/d)$, R_1, s'_1, and α_1 are again given by (A7) and (A8), whereas it results:

$$R_2 = \sqrt{d^2 + b'^2 + 2b'd\sin\vartheta - c'^2}; \quad s'_2 = b + 2b' + \left(c + c'\right)(\pi/2) + c'\alpha_2 \quad \text{(A9)}$$

$$\alpha_2 = \tan^{-1}\left(R_2/c'\right) - \tan^{-1}\left[(d\sin\vartheta + b')/|d\cos\vartheta|\right] \quad \text{(A10)}$$

At last, when $\vartheta_D < \vartheta \leq \pi$, R_2, s'_2, and α_2 are again given by (A9) and (A10), whereas it results:

$$R_1 = \sqrt{d^2 + b'^2 - 2b'd\sin\vartheta - c'^2}; \quad s'_1 = b + c(\pi/2) + c'(\pi/2 - \alpha_1) \quad \text{(A11)}$$

$$\alpha_1 = \tan^{-1}\left(R_1/c'\right) - \tan^{-1}\left[(b' - d\sin\vartheta)/|d\cos\vartheta|\right] \quad \text{(A12)}$$

REFERENCES

1. Gillespie, E. S., "Special issue on near-field scanning techniques," *IEEE Trans. on Antennas and Propagat.*, Vol. 36, 727–901, Jun. 1988.
2. Yaghjian, A. D., "An overview of near-field antenna measurements," *IEEE Trans. on Antennas and Propagat.*, Vol. 34, 30–45, Jan. 1986.
3. Francis, M. H. and R. W. Wittmann, "Near-field scanning measurements: theory and practice," *Modern Antenna Handbook*, C. A. Balanis (ed.), Chapter 19, John Wiley & Sons, Inc., Hoboken, NJ, 2008.
4. Gennarelli, C., A. Capozzoli, L. Foged, J. Fordham, and D. J. van Rensburg, "Special issue on recent advances in near-field to far-field transformation techniques," *Int. Jour. of Antennas and Propagat.*, Vol. 2012.
5. Bucci, O. M., C. Gennarelli, and C. Savarese, "Representation of electromagnetic fields over arbitrary surfaces by a finite and nonredundant number of samples," *IEEE Trans. on Antennas and Propagat.*, Vol. 46, 351–359, Mar. 1998.
6. Bucci, O. M. and C. Gennarelli, "Application of nonredundant sampling representations of electromagnetic fields to NF-FF transformation techniques," *Int. Jour. of Antennas and Propagat.*, Vol. 2012, ID 319856, 14 pages, 2012.

7. Bucci, O. M., F. D'Agostino, C. Gennarelli, G. Riccio, and C. Savarese, "NF-FF transformation with plane-polar scanning: Ellipsoidal modelling of the antenna," *Automatika*, Vol. 41, 159–164, 2000.
8. D'Agostino, F., C. Gennarelli, G. Riccio, and C. Savarese, "Data reduction in the NF-FF transformation with bi-polar scanning," *Microw. Opt. Technol. Lett.*, Vol. 36, 32–36, Jan. 2003.
9. Ferrara, F., C. Gennarelli, R. Guerriero, G. Riccio, and C. Savarese, "An efficient near-field to far-field transformation using the planar wide-mesh scanning," *Journal of Electromagnetic Waves and Applications*, Vol. 21, No. 3, 341–357, 2007.
10. Bucci, O. M., C. Gennarelli, G. Riccio, and C. Savarese, "NF-FF transformation with cylindrical scanning: An effective technique for elongated antennas," *IEE Proc. — Microw., Antennas and Propagat.*, Vol. 145, 369–374, Oct. 1998.
11. D'Agostino, F., F. Ferrara, C. Gennarelli, G. Riccio, and C. Savarese, "NF-FF transformation with cylindrical scanning from a minimum number of data," *Microw. Opt. Technol. Lett.*, Vol. 35, 264–270, Nov. 2002.
12. Bucci, O. M., F. D'Agostino, C. Gennarelli, G. Riccio, and C. Savarese, "Data reduction in the NF-FF transformation technique with spherical scanning," *Journal of Electromagnetic Waves and Applications*, Vol. 15, No. 6, 755–775, 2001.
13. D'Agostino, F., F. Ferrara, C. Gennarelli, R. Guerriero, and M. Migliozzi, "Effective antenna modellings for NF-FF transformations with spherical scanning using the minimum number of data," *Int. Jour. of Antennas and Propagat.*, Vol. 2011, Article ID 936781, 11 pages, 2011.
14. Paris, D. T., W. M. Leach, Jr., and E. B. Joy, "Basic theory of probe-compensated near-field measurements," *IEEE Trans. on Antennas and Propagat.*, Vol. 26, 373–379, May 1978.
15. Leach, W. M., Jr. and D. T. Paris, "Probe compensated near-field measurements on a cylinder," *IEEE Trans. on Antennas and Propagat.*, Vol. 21, 435–445, Jul. 1973.
16. Hansen, J. E., *Spherical Near-field Antenna Measurements*, IEE Electromagnetic Waves Series, Peter Peregrinus, London, UK, 1998.
17. Yaccarino, R. G., L. I. Williams, and Y. Rahmat-Samii, "Linear spiral sampling for the bipolar planar antenna measurement technique," *IEEE Trans. on Antennas and Propagat.*, Vol. 44, 1049–1051, Jul. 1996.

18. Bucci, O. M., F. D'Agostino, C. Gennarelli, G. Riccio, and C. Savarese, "Probe compensated far-field reconstruction by near-field planar spiral scanning," *IEE Proc. — Microw., Antennas and Propagat.*, Vol. 149, 119–123, Apr. 2002.
19. D'Agostino, F., F. Ferrara, C. Gennarelli, R. Guerriero, and M. Migliozzi, "An effective NF-FF transformation technique with planar spiral scanning tailored for quasi-planar antennas," *IEEE Trans. on Antennas and Propagat.*, Vol. 56, 2981–2987, Sep. 2008.
20. D'Agostino, F., F. Ferrara, C. Gennarelli, R. Guerriero, and M. Migliozzi, "Laboratory tests assessing the effectiveness of the NF-FF transformation with helicoidal scanning for electrically long antennas," *Progress In Electromagnetics Research*, Vol. 98, 375–388, 2009.
21. D'Agostino, F., F. Ferrara, J. A. Fordham, C. Gennarelli, R. Guerriero, M. Migliozzi, G. Riccio, and C. Rizzo, "An effective near-field-far-field transformation technique for elongated antennas using a fast helicoidal scan," *IEEE Antennas Propagat. Magazine*, Vol. 51, 134–141, Aug. 2009.
22. D'Agostino, F., F. Ferrara, C. Gennarelli, R. Guerriero, and M. Migliozzi, "Experimental results validating the near-field to far-field transformation technique with helicoidal scan," *The Open Electrical & Electronic Eng. Jour.*, Vol. 4, 10–15, 2010.
23. Bucci, O. M., F. D'Agostino, C. Gennarelli, G. Riccio, and C. Savarese, "NF-FF transformation with spherical spiral scanning," *IEEE Antennas Wireless Propagat. Lett.*, Vol. 2, 263–266, 2003.
24. D'Agostino, F., C. Gennarelli, G. Riccio, and C. Savarese, "Theoretical foundations of near-field-far-field transformations with spiral scannings," *Progress In Electromagnetics Research*, Vol. 61, 193–214, 2006.
25. D'Agostino, F., F. Ferrara, J. A. Fordham, C. Gennarelli, R. Guerriero, and M. Migliozzi, "An experimental validation of the near-field-far-field transformation with spherical spiral scan," *IEEE Antennas Propagat. Magazine*, Vol. 55, Jun. 2013.
26. D'Agostino, F., F. Ferrara, C. Gennarelli, R. Guerriero, M. Migliozzi, and G. Riccio, "A nonredundant near-field to far-field transformation with spherical spiral scanning for nonspherical antennas," *The Open Electrical & Electronic Eng. Jour.*, Vol. 3, 4–11, 2009.
27. D'Agostino, F., F. Ferrara, C. Gennarelli, R. Guerriero, and M. Migliozzi, "Experimental assessment of an effective near-field-far-field transformation with spherical spiral scanning for

quasi-planar antennas," *IEEE Antennas Wireless Propagat. Lett.*, Vol. 12, 670–673, 2013.

28. D'Agostino, F., F. Ferrara, C. Gennarelli, R. Guerriero, and M. Migliozzi, "Far-field reconstruction from a minimum number of spherical spiral data using effective antenna modellings," *Progress In Electromagnetics Research B*, Vol. 37, 43–58, 2012.
29. D'Agostino, F., F. Ferrara, C. Gennarelli, R. Guerriero, and M. Migliozzi, "The unified theory of near-field-far-field transformations with spiral scannings for nonspherical antennas," *Progress In Electromagnetics Research B*, Vol. 14, 449–477, 2009.
30. D'Agostino, F., F. Ferrara, C. Gennarelli, G. Gennarelli, R. Guerriero, and M. Migliozzi, "On the direct non-redundant near-field-to-far-field transformation in a cylindrical scanning geometry," *IEEE Antennas Propagat. Magazine*, Vol. 54, 130–138, Feb. 2012.
31. D'Agostino, F., F. Ferrara, C. Gennarelli, G. Gennarelli, R. Guerriero, and M. Migliozzi, "Antenna pattern reconstruction directly from nonredundant near-field measurements collected by a cylindrical facility," *Progress In Electromagnetics Research M*, Vol. 24, 235–249, 2012.
32. D'Agostino, F., F. Ferrara, C. Gennarelli, R. Guerriero, and M. Migliozzi, "An innovative direct NF-FF transformation technique with helicoidal scanning," *Int. Jour. of Antennas and Propagat.*, Vol. 2012, Article ID 912948, 9 pages, 2012.
33. D'Agostino, F., F. Ferrara, C. Gennarelli, R. Guerriero, and M. Migliozzi, "Evaluation of the far field radiated by long antennas directly from data acquired through a fast helicoidal scanning," *Progress In Electromagnetics Research M*, Vol. 26, 157–171, 2012.
34. Wacker, P. F., *Non-planar Near-field Measurements: Spherical Scanning*, NBSIR 75-809, Boulder, CO, 1975.
35. Yaghjian, A. D. and R. C. Wittmann, "The receiving antenna as a linear differential operator: Application to spherical near-field measurements," *IEEE Trans. on Antennas and Propagat.*, Vol. 33, 1175–1185, 1985.
36. Hansen, T. B., "Higher-order probes in spherical near-field scanning," *IEEE Trans. on Antennas and Propagat.*, Vol. 59, 4049–4059, Nov. 2011.
37. Bucci, O. M., G. D'Elia, and M. D. Migliore, "Advanced field interpolation from plane-polar samples: Experimental verification," *IEEE Trans. on Antennas and Propagat.*, Vol. 46, 204–210, Feb. 1998.